ACS APPLIED MATERIALS & INTERFACES

www.acsami.org

Research Article

Ytterbium-Doped $CsPbCl_3$ Quantum Cutters for Near-Infrared Light-Emitting Diodes

Hai Huang,[▽] Renfu Li,[▽] Shilin Jin, Zhifang Li,* Ping Huang, Jinquan Hong, Shaowu Du, Wei Zheng, Xueyuan Chen,* and Daqin Chen*

Cite This: *ACS Appl. Mater. Interfaces* 2021, 13, 34561−34571

Read Online

ACCESS | Metrics & More | Article Recommendations | Supporting Information

ABSTRACT: Exploring highly efficient near-infrared (NIR) emitting materials is desirable for the advancement of next-generation smart NIR light sources. Different from most reported Cr^{3+}-doped emitters with far-red emissions, Yb^{3+}-activated phosphors are expected to yield pure NIR (~1000 nm) light. Herein, a new hot-injection route using all metal-oleate salts to fabricate Yb^{3+}-doped $CsPbCl_3$ perovskite nanocrystals (PeNCs) is reported for the first time, which produce PeNC-sensitized Yb^{3+} NIR emission with photoluminescence quantum yields (PLQYs) higher than 100%. With the help of temperature-dependent PL spectra, femtosecond transient absorption spectra, and time-resolved PL spectra, it is evidenced that the in situ produced intrinsic shallow trap states in a $CsPbCl_3$ host play a key role in facilitating the picosecond nonradiative cooperative energy transfer from PeNCs to two Yb^{3+} dopants simultaneously. Using the optimized Yb^{3+}:$CsPbCl_3$ quantum cutters, a phosphor-converted NIR light-emitting diode (pc-NIR-LED) is fabricated, exhibiting an external quantum efficiency of 2%@28 mA, a high NIR output irradiance of 112 mW/cm^2@400 mA, and excellent long-term stability. Finally, the designed pc-NIR-LED is demonstrated to have great potential as an invisible night-vision light source.

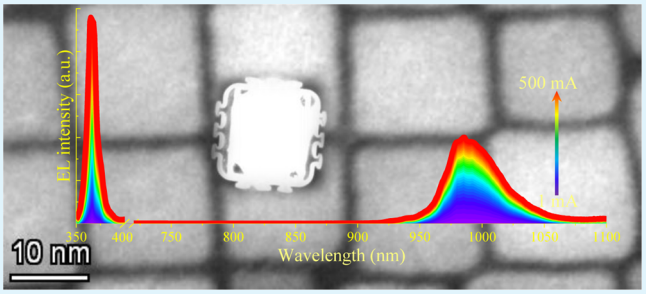

KEYWORDS: *NIR-LED, Yb^{3+} dopants, quantum cutting, perovskite quantum dots, $CsPbCl_3$*

INTRODUCTION

Near-infrared (NIR) light-emitting diodes (LEDs) have recently attracted considerable attention due to their promising applications in night-vision lighting, optical communication, bioimaging, medical diagnostics, and food analysis.[1−4] In this regard, NIR-emitting phosphor-converted LEDs (pc-LEDs), generally constructed by coupling commercial blue InGaN LED chip and NIR phosphors, show the advantages of small size, cost-effective fabrication, and high output power/efficiency.[5,6] Therefore, NIR luminescent materials play a crucial role in the overall performance of NIR-LED devices. At present, Cr^{3+}-doped inorganic phosphors have been regarded as desirable NIR emitters, which can yield either narrowband (sharp-line) or broadband NIR emission depending on the doping hosts.[7] Although great progress has been made in this field, most reported Cr^{3+} emissions with high photoluminescence quantum yields (PLQYs) are actually located in the far-red region visible to the naked eyes (the central wavelengths of 700−800 nm)[8−14] rather than the NIR one (especially for emission wavelengths over 900 nm),[15] which remarkably limits their practical applications.

As one of the most important lanthanide dopants, Yb^{3+}-activated phosphors generally possess high PLQYs and can produce genuine and usable broadband NIR light with a peak wavelength of ~1000 nm.[16] However, the parity-forbidden 4f−4f transition of Yb^{3+} leads to weak light absorption and its 4f[13] electronic configuration can only produce two manifolds, i.e., the $^2F_{7/2}$ ground state and the $^2F_{5/2}$ excited state, which makes it impossible to be pumped by the widely used commercial ultraviolet (UV) or blue LED chips. As an alternative, sensitizing Yb^{3+} emission via semiconductor quantum dots (QDs) is an effective strategy to address this tough issue owing to the allowed and efficient band−band absorption of QDs and their tunable bandgaps.[17] Indeed, Yb-doped $CsPb(Cl/Br)_3$ perovskite QDs (PeQDs) or perovskite nanocrystals (PeNCs) have been recently reported, which can produce quantum cutting luminescence with PLQYs higher than unity via efficient energy transfer from PeNCs to Yb^{3+} dopants.[18−20] This feature is quite different for all previous Ln-based quantum cutters[21−25] due to its strong and broadband absorption in the UV-blue energy region relevant for quantum cutting, which enables Yb^{3+}:$CsPbCl_3$ PeNCs to find promising applications in photovoltaics by harvesting solar photons.[26−30]

Received: May 21, 2021
Accepted: July 8, 2021
Published: July 19, 2021

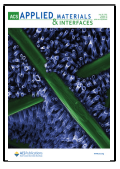

In this work, we aim to expand the application of Yb^{3+}:$CsPbCl_3$ PeNCs in NIR pc-LED devices. The Yb^{3+}-doped $CsPbCl_3$ PeNCs are conveniently fabricated by employing all metal-oleate salts as cation precursors for the first time, which can produce PeNC-sensitized Yb^{3+} NIR emission with PLQYs higher than 100%. The constructed quantum cutter-converted NIR-LED exhibits an external quantum efficiency (EQE) of 2%@28 mA, a high NIR output irradiance of 112 mW/cm^2@400 mA, and superior long-term operation stability, showing potential as an invisible night-vision light source.

EXPERIMENTAL SECTION

Materials. 1-Octadecene (ODE, Aladdin, 90%), oleic acid (OA, Aldrich, 90%), olyelamine (OM, Aladdin, 80−90%), lead nitrate ($Pb(NO_3)_2$, Macklin, 99.99%), ytterbium nitrate ($Yb(NO_3)_3{\cdot}6H_2O$, Macklin, 99.99%), Cs_2CO_3 (Aladdin, 99.9%), potassium oleate (KOA, Aladdin, 98%), trimethylchlorosilane (TMS-Cl, Macklin 99%), trimethylbromosilane (TMS-Br, Macklin 99%), hexane (Aladdin, 99%), and toluene (Sinopharm Chemical Reagent Co. Ltd., 99%). All chemicals were used without further purification.

Synthesis of Cs-Oleate (CsOA). Cs_2CO_3 (0.8 g) was loaded into a mixture containing 30 mL of ODE and 2.5 mL of OA and then heated to 200 °C until the white powder was completely dissolved. Then, the mixture was maintained at 130 °C for 1 h under vacuum. During the synthesis of PeNCs, the CsOA solution should be heated to 130 °C to avoid precipitation.

Synthesis of Ytterbium-Oleate ($Yb(OA)_3$) and Lead-Oleate ($Pb(OA)_2$). $Yb(NO_3)_3{\cdot}6H_2O$ (1.868 g) was dissolved in 20 mL of deionized H_2O to form solution A; 4.0 g of KOA was ultrasonically dissolved in 20 mL of deionized H_2O and 25 mL of ethanol to form solution B. Then solutions A and B were thoroughly mixed. Excess cyclohexane (50 mL) was added to extract $Yb(OA)_3$ by continuously stirring for 20 min. The upper organic layer was separated, cyclohexane was distilled off, and the residue was washed with water and dried to obtain the $Yb(OA)_3$ product. $Pb(OA)_2$ can be prepared in a similar way using $Pb(NO_3)_2$ as the precursor.

Synthesis of Yb^{3+}:$CsPbCl_3$ PeNCs and Purification. Briefly, 10 mL of ODE, 1 mL of OM, 3 mL of OA, 0.2 mmol of $Pb(OA)_2$, 200 μL of 1 M CsOA in ethanol, and 0.09 mmol of $Yb(OA)_3$ were added to a 50 mL round bottom flask. The solution was stirred and flushed with N_2, kept at 160 °C for 0.5 h, and then heated to 240 °C. Upon reaching this temperature, 0.2 mL of TMS-Cl in 0.5 mL of ODE was swiftly injected. Immediately after injection, the flask was cooled to room temperature using a water bath. The crude nanocrystal solution was centrifuged at 1300 rpm for 15 min. The supernatant was discarded and the pellet was resuspended in hexanes. The PeNCs were then washed with ethyl acetate. The solution was then centrifuged at 1300 rpm for 10 min. The supernatant was discarded, and the pellet was resuspended in hexanes.

Synthesis of Yb^{3+}:$CsPb(Cl/Br)_3$ PeNCs. The procedure is similar to that for Yb^{3+}:$CsPbCl_3$ except that 0.2 mL of TMS-Cl was partially substituted by TMS-Br.

Construction of Yb^{3+}:$CsPbCl_3$ Quantum Cutter-Based NIR-LED. The device was constructed by directly coupling the as-fabricated Yb^{3+}:$CsPbCl_3$ quantum cutters on the InGaN UV chip. The Yb^{3+}:$CsPbCl_3$ PeNCs were homogeneously dispersed in the mixture of A/B gels (1:1, k-9761, Kafuter, Guangzhou Hengda New Material Co., Ltd) and then dropped on the chip. The major component of the A gel is epoxy resin and that of B gel is the curing agent. Additionally, opaque silica gels were filled around the edges of the device to avoid the leakage of UV light. The emitting area of pc-NIR-LED is 0.06 cm^2.

General Characterization. X-ray diffraction (XRD) analysis was carried out to identify Yb^{3+}:$CsPbCl_3$ phase structures using a Bruker D8 Advance X-ray powder diffractometer with Cu Kα radiation (λ = 0.154 nm) operating at 40 kV. Microstructure observations of Yb-doped $CsPbCl_3$ PeNCs were performed on a JEOL JEM-2010 transmission electron microscope (TEM) operated at 200 kV accelerating voltage equipped with an energy dispersive X-ray (EDX) spectroscopy system. Scanning TEM (STEM) images and elemental maps were recorded on an FEI aberration-corrected Titan Cubed S-Twin microscope operated in high-angle annular dark-field (HAADF) mode. The actual chemical compositions were determined by inductively coupled plasma mass spectroscopy (ICP-MS) using a Perkin-Elmer Optima 3300DV spectrometer. The optical absorption spectra were recorded on a spectrophotometer (Lambda900, Perkin-Elmer) with a resolution of 1 nm. PL spectra and Yb^{3+} decay curves were recorded on an Edinburgh Instruments FLS1000 spectrofluorometer equipped with a 450 W xenon lamp and 60 W pulse xenon lamp as the excitation sources. Time-resolved spectra for exciton recombination were detected on a fluorescent lifetime spectrometer (Edinburgh Instruments, LifeSpec-II) based on a time-correlated single photon counting technique under excitation of a 375 nm picosecond laser. PLQY, defined as the ratio of emitted photons to absorbed ones, was determined with a spectrofluorometer (FLS1000) equipped with a xenon lamp as the excitation source and a 15 cm integrating sphere. Temperature-dependent PL spectra were measured on an Edinburgh Instruments FLS980 spectrofluorometer equipped with a Linkam THMS600 temperature controlling stage. The luminance (L)−current density (J)−voltage (V) characteristics were collected using a Keithley 2400 source. The electroluminescence (EL) spectra and light output parameters of the UV LED chip and the fabricated pc-NIR-LED were measured using a fiber integration sphere and a PMA-12 spectrometer.

Laser Power-Dependent NIR Emissions. A 375 nm picosecond pulsed (20 MHz) laser diode was used as the excitation source. The excitation beam was collimated to a diameter of ∼1 mm and directed to the Yb^{3+}:$CsPbCl_3$ sample at an angle of ∼90° from the collection axis. Irradiance was adjusted by passing the excitation beam through a variable neutral density filter wheel and additional neutral density filters as required. Laser powers between 10^{-3} and 10^{-1} mW were measured with a dual-channel optical power and energy meter (THORLABS, PM320E). The NIR PL spectra were recorded on an Edinburgh Instruments FLS1000 spectrofluorometer.

Transient Absorption (TA) Spectroscopy. TA data were collected with a HARPIA spectroscopy system. The laser from a commercial diode-pumped Yb:KGW laser system (PHAROS, Light Conversion) operating at 8.9 kHz and 1030 nm, with ∼0.2 mJ maximum pulse energy and ∼200 fs pulse width was split into two beams. One beam was used to pump an optical parametric amplifier (ORPHEUS, Light Conversion) and the second harmonic generation (LYRA, Light Conversion), which generated the tunable pump pulses (315−2700 nm). The central wavelength of the pump pulse used in this work was 360 nm, and the power of the pump pulse was attenuated by neutral density filters. Another beam first passed through an BBO crystal to generate 515 nm pump beam, and then focused on a Ti:Sapphire crystal to generate the broadband probe pulses (350−750 nm). Time delays of up to ∼8 ns were achieved via an optical delay line. Colloidal PeNCs dispersed in hexane were placed in a sealed 2 mm path length quartz cuvette equipped with a Teflon stir bar. The pulse energy density of the pump pulse was reduced to 0.07 μJ/cm^2 to prevent sample degradation/photocharging so that scan-to-scan kinetics did not appreciably change with prolonged laser exposure.

RESULTS AND DISCUSSION

Currently, the hot-injection route is a well-known technique for synthesizing PeNCs including $CsPbCl_3$. However, to fabricate Yb^{3+}-doped perovskite NCs, the selection of precursor salts is important to realize the incorporation of Yb^{3+} dopants into the $CsPbCl_3$ lattice and obtain pure Yb:$CsPbCl_3$ phase. In the previous works, metal chlorides ($PbCl_2$, $YbCl_3$)[18] or metal acetates ($Pb(CH_3CO_2)_2$, Yb-$(CH_3CO_2)_3$)[19] have been used. Unfortunately, the synthesis in our lab was met with difficulties associated with the

https://doi.org/10.1021/acsami.1c09421
ACS Appl. Mater. Interfaces 2021, 13, 34561−34571

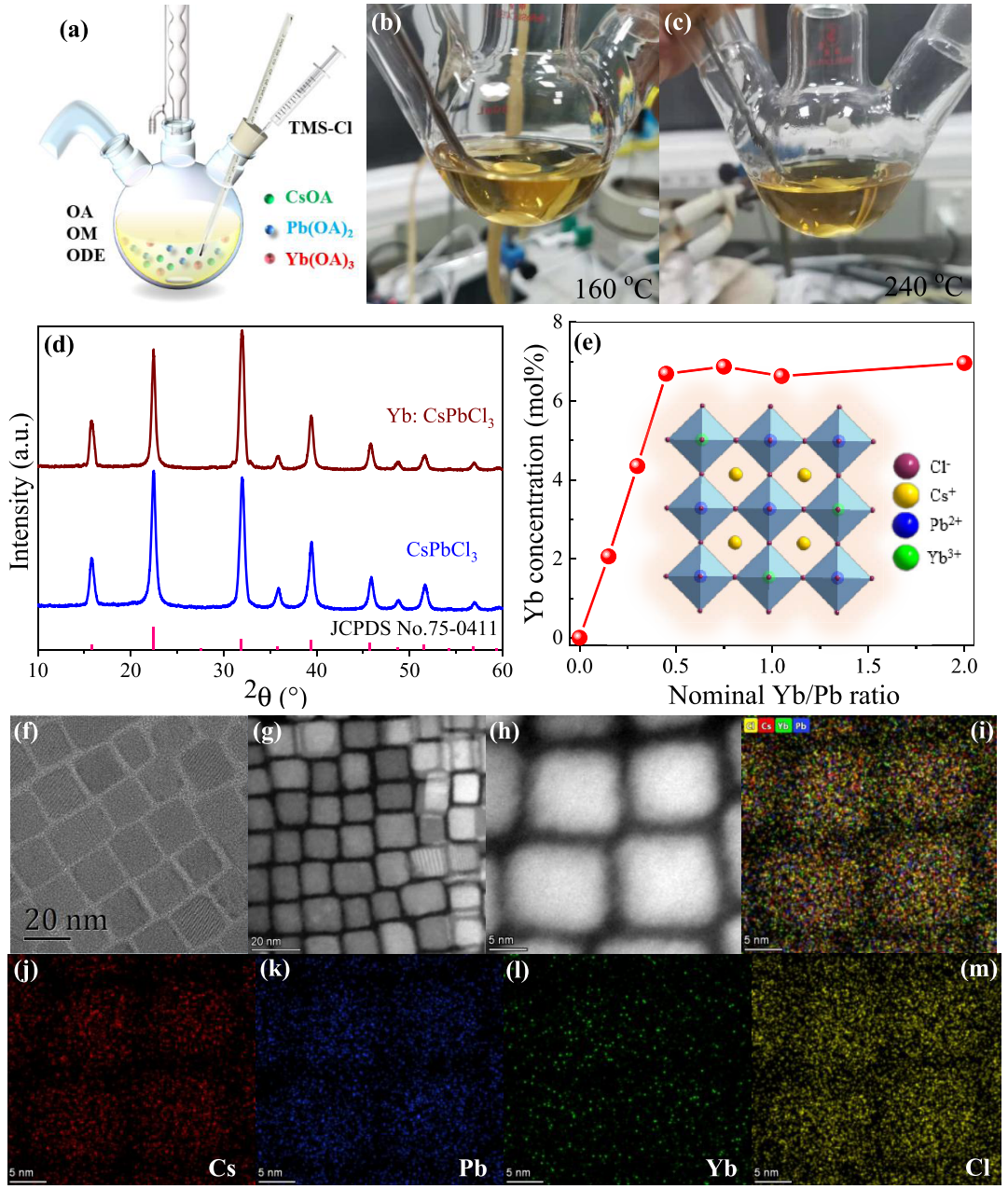

Figure 1. (a) Schematic illustration of the synthesis procedure for the Yb-doped $CsPbCl_3$ PeNCs and the reaction solution upon heating at temperatures of (b) 160 °C and (c) 240 °C. (d) XRD patterns of undoped and Yb-doped $CsPbCl_3$ samples. Bars represent standard diffraction data of the cubic $CsPbCl_3$ phase (JCPDS No. 75-0411). (e) Dependence of Yb^{3+} doping content in $CsPbCl_3$ on the nominal Yb/Pb feeding ratio. Inset is the schematic illustration of the Yb-doped $CsPbCl_3$ crystal structure. (f) HRTEM and (g, h) HAADF-STEM images of Yb^{3+}:$CsPbCl_3$ PeNCs and (i–m) the corresponding EDX elemental mapping of Cs, Pb, Yb, and Cl.

precipitation of undesired impurities (Figures S1 and S2) when the reaction temperature was increased up to 240 °C to induce Yb^{3+} doping. Herein, we report an alternative approach to fabricate Yb^{3+}:$CsPbCl_3$ PeNCs by employing all metal-oleate salts (CsOA, $Pb(OA)_2$, and $Yb(OA)_3$) as the cation precursors and TMS-Cl as the anion precursor, respectively (Figure 1a). In this case, the OA/OM/ODE solution containing Cs^+, Pb^{2+}, and Yb^{3+} ions remain transparent with the increase of temperature from 160 to 240 °C (Figure 1b,c) owing to the shortage of anion sources in the solution, indicating that the solution at high reaction temperature (240 °C) is stable without formation of any impurities. Upon the injection of TMS-Cl, pure Yb^{3+}:$CsPbCl_3$ precipitates are quickly produced within a few seconds.

XRD patterns (Figure 1d) evidence that the products are in agreement with the cubic $CsPbCl_3$ phase (JCPDS No. 75-0411). Introducing Yb^{3+} dopants will not induce the formation of impurity phases. ICP-MS data confirm the incorporation of Yb^{3+} ions into the $CsPbCl_3$ host. With the increase of the Yb/Pb nominal feeding ratio, Pb^{2+} ions are gradually replaced by Yb^{3+} dopants, and Yb^{3+} concentration can reach as high as ~7 mol % (Figure 1e). Afterward, further increasing Yb/Pb feeding ratio will not lead to a higher Yb^{3+} content in the $CsPbCl_3$ host, indicating the occurrence of doping saturation (Figure 1e). High-resolution TEM (HRTEM) images (Figures

https://doi.org/10.1021/acsami.1c09421
ACS Appl. Mater. Interfaces 2021, 13, 34561−34571

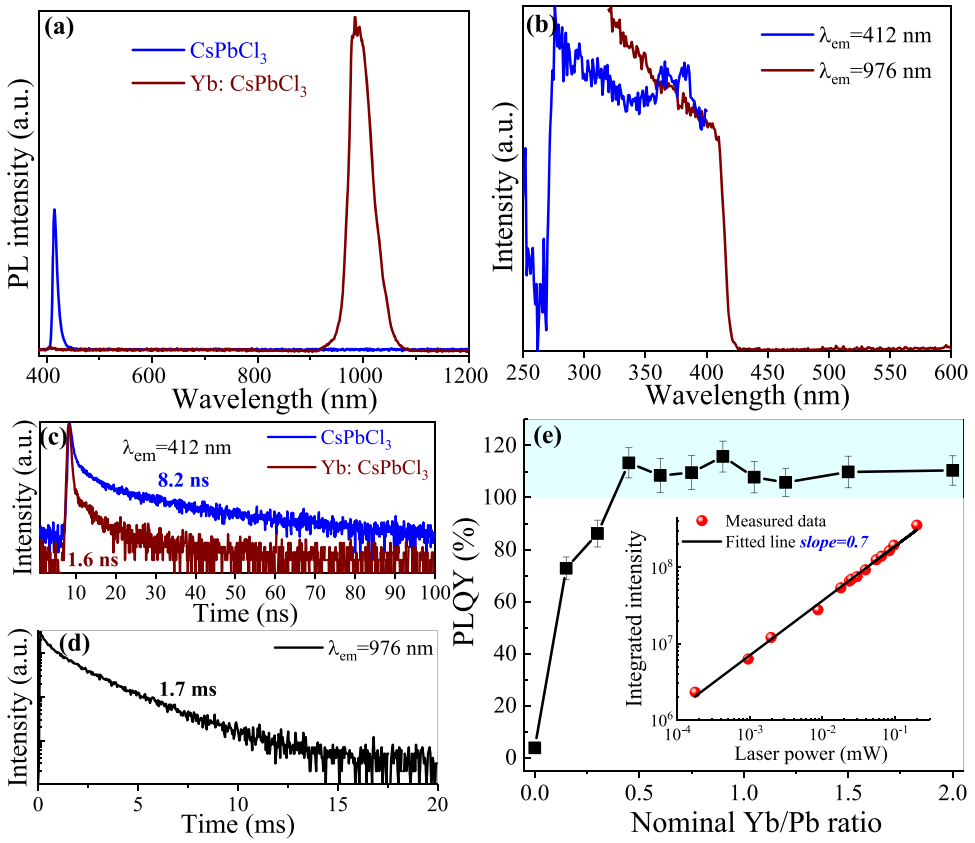

Figure 2. (a) PL spectra of $CsPbCl_3$ and Yb^{3+}:$CsPbCl_3$ PeNCs. (b) PLE spectra of Yb^{3+}:$CsPbCl_3$ PeNCs by monitoring visible exciton recombination emission (λ_{em} = 412 nm) and Yb^{3+} NIR emission (λ_{em} = 976 nm). PL decay curves of Yb^{3+}:$CsPbCl_3$ PeNCs by recording (c) exciton recombination (λ_{em} = 412 nm) and (d) NIR emission (λ_{em} = 976 nm). (e) Dependence of PLQYs on the nominal Yb/Pb feeding ratio. Inset is the log−log plot of NIR emission intensity versus photoexcitation power from a 375 nm picosecond pulsed (20 MHz) laser diode.

1f and S3) present the pure cubic shape of PeNCs with uniform size distribution (~15 nm) and high crystallinity (distinctly resolved lattice fringes). HAADF-STEM images (Figure 1g,1h) together with EDX elemental mappings (Figures 1i−m and S4) of Yb^{3+}:$CsPbCl_3$ PeNCs demonstrate the homogeneous distribution of Cs, Pb, Cl, and Yb signals. Elemental analyses confirm that Yb^{3+} dopants are indeed located in the $CsPbCl_3$ lattice and the atomic percentage with respect to Pb^{2+} is ~7% for the product prepared with Yb/Pb = 0.45 (Figure S5), which agrees well with ICP-MS results.

The PL spectrum for the pristine $CsPbCl_3$ PeNCs (Figure 2a) shows narrow violet (~412 nm) band-edge luminescence assigned to exciton recombination under UV excitation. Incorporating Yb^{3+} activators into $CsPbCl_3$ leads to extra broadband NIR luminescence (~976 nm) attributed to 4f−4f electron transition of Yb^{3+}:$^2F_{5/2} \rightarrow {}^2F_{7/2}$ (Figure 2a). Notably, the 412 nm band-edge luminescence in Yb^{3+}:$CsPbCl_3$ is almost quenched, and PL excitation (PLE) spectra by monitoring both violet and NIR emissions (Figure 2b) as well as absorption spectra (Figure S6) exhibit similar band-edge absorption features, indicating efficient PeNCs to Yb^{3+} energy transfer. Indeed, time-resolved emission spectra illustrate faster deexcitation of excitons upon Yb^{3+} doping (Figure 2c), and the mean lifetime remarkably decreases from 8.2 to 1.6 ns owing to the extra nonradiative energy transfer decay channel from PeNCs to Yb^{3+} dopants. Notably, the decay lifetime for exciton recombination of PeNCs is in a nanosecond scale for its allowed transition,[31] while the decay curve of Yb^{3+} emission (Figure 2d) exhibits a typical parity-forbidden 4f−4f transition with a long lifetime on a millisecond scale (~1.7 ms).[32]

To explore the synthetic conditions for Yb^{3+}:$CsPbCl_3$ with the best performance, a series of comparison experiments were performed. As demonstrated in Figures S7−S9, the reaction temperature, and the OA/OM contents play key roles in promoting the incorporation of Yb^{3+} dopants into the $CsPbCl_3$ host. The optimal reaction temperature is 240 °C (Figure S7) and the OA/OM contents are 3 and 1 mL, respectively (Figures S8 and S9). Interestingly, Cs/Pb feeding ratio has no remarkable influence on Yb^{3+} doping (Figure S10) and the critical Yb/Pb feeding ratio is 0.45 (Figure S11). Above this value, no obvious change in PL intensity is observed owing to the Yb^{3+} doping saturation, which is consistent with the ICP-MS results. In this regard, we measured the PLQYs of the Yb^{3+}:$CsPbCl_3$ solid-state powders prepared under the optimal reaction conditions and varied Yb/Pb feeding ratios (Figure S12). The change in PLQYs (Figure 2e) agrees well with that of ICP-MS results, and the PLQYs are invariable and surpass unity (~110%) when the Yb/Pb ratio reaches the critical value of 0.45. Over 100% PLQYs for the present Yb^{3+}:$CsPbCl_3$ samples indicate that the energy transfer from PeNCs to Yb^{3+} dopants is a typical quantum cutting process, which is similar to the cases previously reported for Yb^{3+}:$CsPbCl_3$ prepared by other methods.[18−20] To further testify this, photoexcitation power-dependent NIR PL spectra of Yb^{3+}:$CsPbCl_3$ were recorded (Figure S13). Theoretically, NIR emission intensity I_{Yb} depends on the excitation power P according to the relationship of $I_{Yb} \propto P^n$, where n is equal to 0.5 for the non-

https://doi.org/10.1021/acsami.1c09421
ACS Appl. Mater. Interfaces 2021, 13, 34561−34571

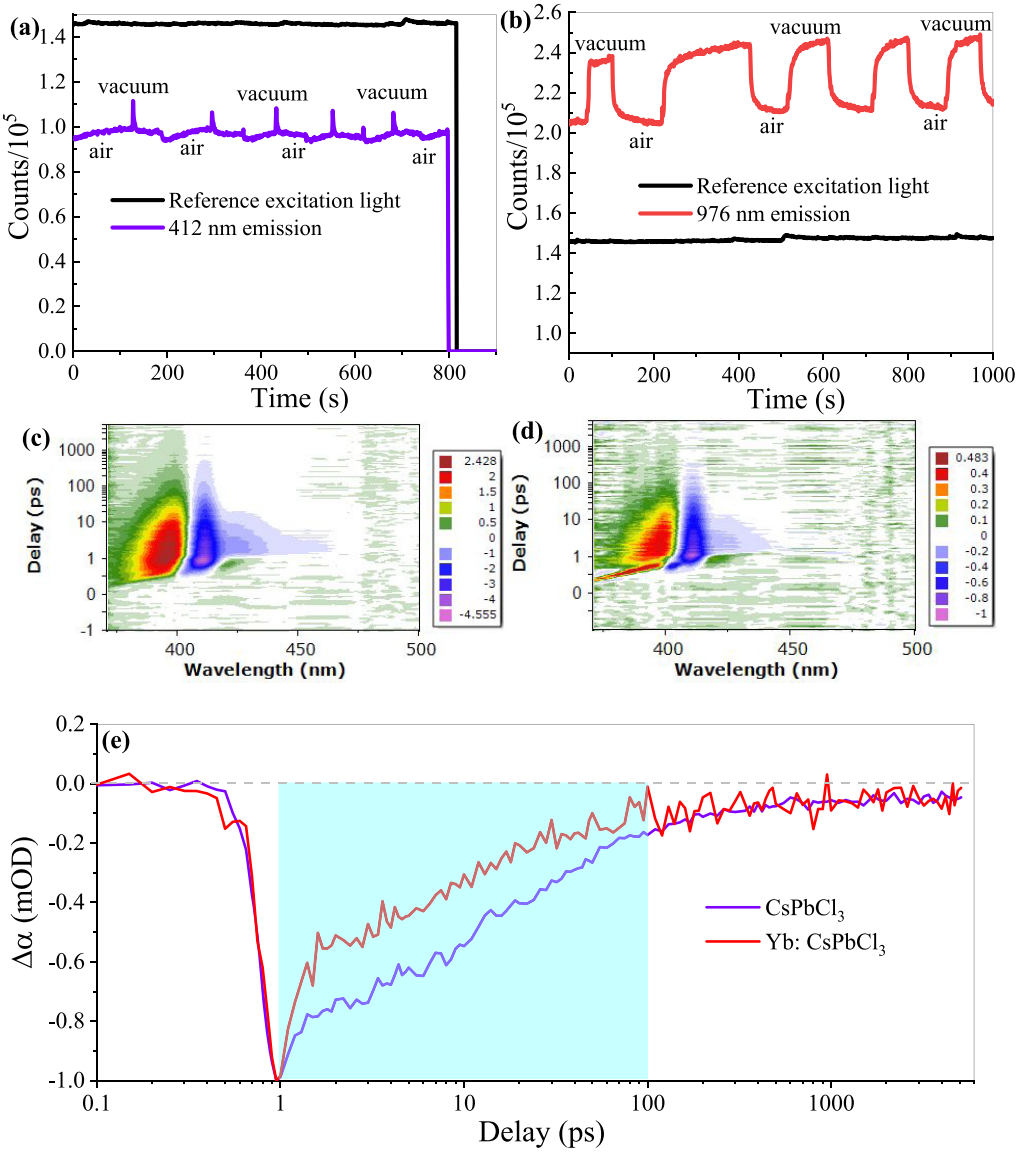

Figure 3. Variation in PL intensity of Yb^{3+}:$CsPbCl_3$ during air−vacuum exchange: (a) 412 nm exciton recombination emission and (b) 976 nm NIR emission of Yb^{3+}. Two-dimensional femtosecond laser pumping transient absorption spectra of (c) $CsPbCl_3$ and (d) Yb^{3+}:$CsPbCl_3$ samples. (e) First-exciton bleach-recovery kinetics measured at room temperature for $CsPbCl_3$ and Yb^{3+}:$CsPbCl_3$ samples.

linear quantum cutting process.[33−35] As shown in Figure 2e, the slope (n) of the double logarithmic plot of NIR integrated intensity versus the pumping laser power is fitted to be 0.7. Such sublinear fitting confirms the dominant quantum cutting luminescence process for the Yb^{3+}:$CsPbCl_3$ sample and the deviation from the theoretical value of 0.5 is probably attributed to the saturation population of Yb^{3+} $^2F_{5/2}$ excited state stemming from its long lifetime.[36]

To further verify PeNC-sensitized energy transfer Yb^{3+} NIR luminescence, we examined the emitting behaviors of $CsPbCl_3$ and Yb^{3+}:$CsPbCl_3$ samples in the air and vacuum surroundings. Both samples show enhanced band-edge and Yb^{3+} NIR emissions accompanied by prolonged decay lifetimes after placing the samples in a vacuum (Figure S14), probably owing to the reduced nonradiative/quenching channels for exciton recombination and PeNCs to Yb^{3+} energy transfer in a vacuum. Interestingly, the alternate air/vacuum environment leads to the cycling change of exciton recombination emission (Figure 3a). Correspondingly, Yb^{3+} NIR emission shows a similar rise/decline variation tendency (Figure 3b), confirming that NIR luminescence has indeed originated from PeNCs to Yb^{3+} energy transfer. To further testify this, the femtosecond time-resolved TA exciton bleach-recovery kinetics recorded on undoped $CsPbCl_3$ and Yb^{3+}:$CsPbCl_3$ samples were investigated, as shown in Figure 3c,d. Both samples showed typical ground state bleach and excited-state absorption. It is clear that the Yb^{3+}:$CsPbCl_3$ sample relative to the undoped $CsPbCl_3$ one exhibits a weaker bleach signal and faster recovery (Figures S15 and 3e). This indicates that there is an extra carrier-trapping channel, from which the exciton energy is transferred to Yb^{3+} dopants. As evidenced in Figure 3e, the exciton trapping time is less than 100 ps, which is much faster than their decay lifetimes (in the nanosecond scale). This ultrafast process ensures efficient PeNCs to Yb^{3+} energy transfer and subsequent NIR quantum cutting emission of Yb^{3+}.

Temperature-dependent PL spectra measured from 10 to 310 K for the $CsPbCl_3$ sample show that the bandgap and spectral broadening increase with temperature (Figure 4a),

https://doi.org/10.1021/acsami.1c09421
ACS Appl. Mater. Interfaces 2021, 13, 34561−34571

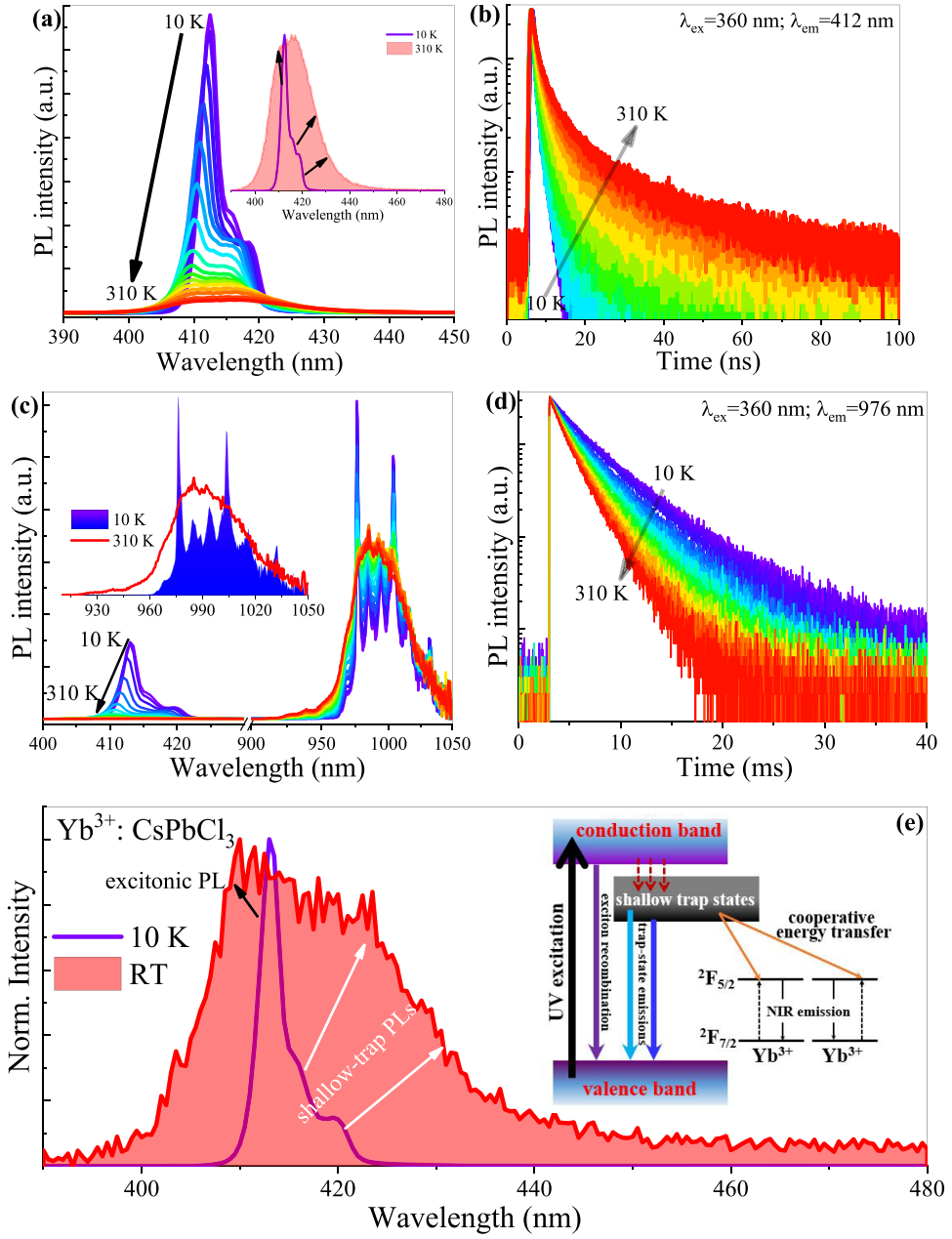

Figure 4. Temperature-dependent (10−310 K) steady-state PL spectra of (a) $CsPbCl_3$ and (c) Yb^{3+}:$CsPbCl_3$. Time-resolved PL spectra by monitoring (b) exciton recombination of $CsPbCl_3$ and (d) Yb^{3+} NIR emission of Yb^{3+}:$CsPbCl_3$. (e) Normalized PL spectra of Yb^{3+}:$CsPbCl_3$ in the wavelength range of 380−480 nm. Inset is the proposed PeNC-sensitized Yb^{3+} quantum cutting luminescence involving shallow-trap state-assisted cooperative energy transfer.

which is widely reported for perovskite semiconductors. Time-resolved PL (TRPL) measurements for exciton recombination are shown in Figure 4b and the fitted decay lifetimes are tabulated in Table S1. As the temperature is increased, the TRPL signals show an increase in the decay time (within the temperature range of 10−310 K, Figure S16). This is mainly attributed to the formation of free carriers with a slower recombination rate, generated from the fission of the bound excitons at higher temperatures.[37] This kinetic behavior is also reflected in the bi-exponential character of TRPL curves, i.e., the higher the temperature, the more obvious the bi-exponential fitting (Table S1).

For Yb^{3+}:$CsPbCl_3$, similar exciton recombination kinetics were observed besides extra NIR emission of Yb^{3+} (Figure 4c). At lower temperatures, NIR emission spectra are highly structured (inset of Figures 4c and S17), assigned to the electron transitions between the crystal-field-split $^2F_{5/2}$ and $^2F_{7/2}$ states. Notably, these Stark splitting peaks from Yb^{3+}:$CsPbCl_3$ PeNCs resemble those from the Yb^{3+}-doped single-crystal,[38] indicating similar crystal-field environments for Yb^{3+} dopants, i.e., the Yb^{3+} activators dominantly locate inside the $CsPbCl_3$ crystal lattice rather than on the PeNC surfaces. Furthermore, different from the case of exciton recombination, TRPL spectra of Yb^{3+} dopants show a monotonous decrease in decay lifetime with increasing temperature (Figures 4d, S16, and Table S2) due to the heating-induced nonradiative deexcitation.

https://doi.org/10.1021/acsami.1c09421
ACS Appl. Mater. Interfaces 2021, 13, 34561−34571

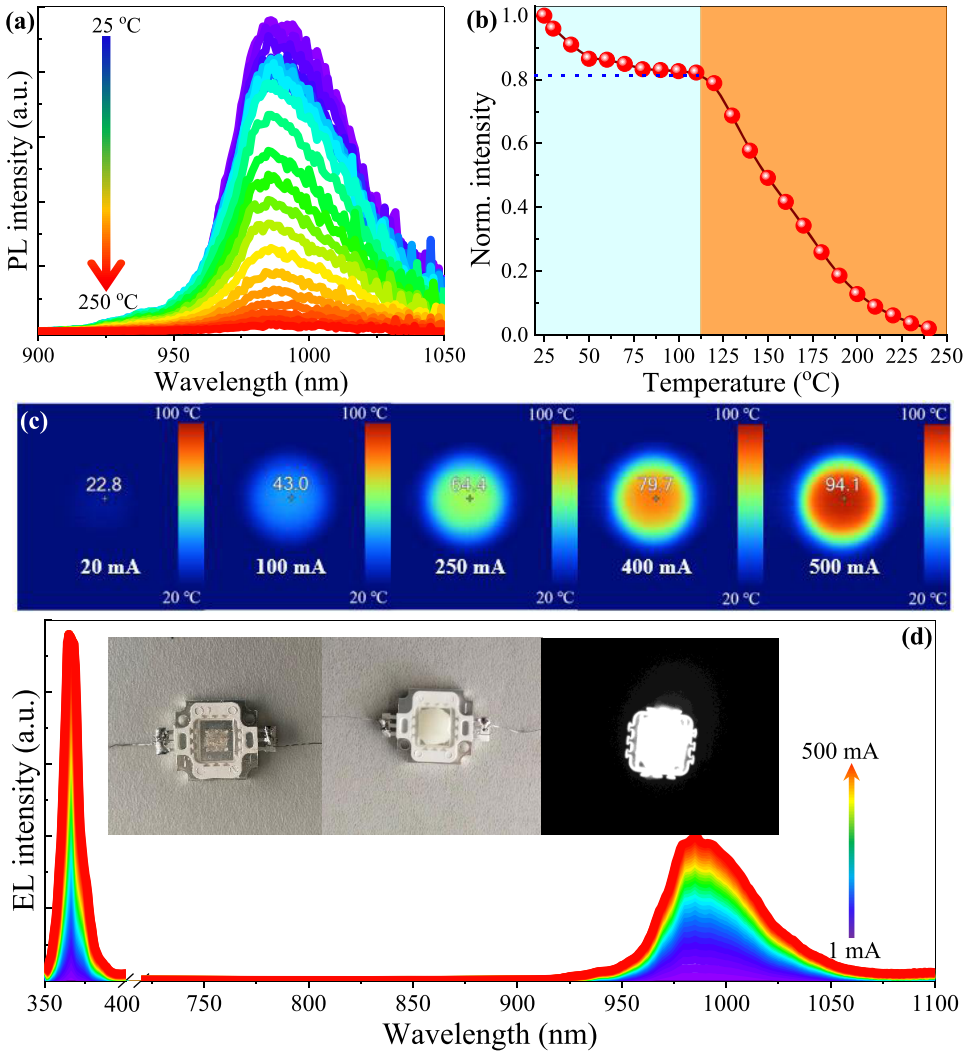

Figure 5. Thermal stability test of NIR emission for the Yb^{3+}:$CsPbCl_3$ phosphor: (a) PL spectra and (b) PL intensity versus temperature. (c) Variation of the actual temperature for the commercial UV LED chip (fixed voltage of 10 V) with the increase of the forward bias current. (d) EL spectra for the pc-NIR-LED device with the increase of the forward bias current from 1 to 500 mA. Insets are the photographs of the UV chip, the constructed pc-NIR-LED, and the working device at 300 mA.

Importantly, in addition to excitonic PL, it is observed that both undoped $CsPbCl_3$ and Yb-doped $CsPbCl_3$ samples actually show multiple shallow-trap-state near-band-edge emissions even at 10 K (inset of Figure 4a,e). These shallow-trap PLs become broadened and intensified at room temperature due to the coupling of vibronic sidebands and hot bands,[37] indicative of in situ formation of intrinsic shallow-trap states for the present samples prepared by using metal-oleates. These features are quite different from those of previously reported Yb^{3+}:$CsPbCl_3$ using metal acetates as the precursors, where extra defect states were produced with the necessity of Yb^{3+} doping. Herein, we propose a possible energy transfer mechanism to produce Yb^{3+} NIR quantum cutting luminescence, as illustrated in the inset of Figure 4e. Upon UV excitation, photogenerated carriers are produced within the conduction band (CB) and then captured by the shallow-trap states, from which the combined multiple-state violet-blue emissions are generated. Upon the introduction of Yb^{3+} dopants into $CsPbCl_3$ PeNCs, the energy will be transferred downstream from the trapped excited state to two Yb^{3+} activators via a one-step cooperative energy transfer. Such cascade energy transfer in Yb^{3+}:$CsPbCl_3$ will lead to efficient NIR luminescence of Yb^{3+} with PLQY higher than unity (i.e., PeNC-sensitized Yb^{3+} quantum cutting luminescence). The present mechanism is different from the ones previously proposed, which involve defect-related intermediate energy state and two-step energy transfer[18] or Yb^{3+}-induced near-band-edge defect state that subsequently transfers energy to two neighboring Yb^{3+} ions in a single concerted step.[19,39]

Furthermore, the anion exchange strategy is used to modify the bandgaps of Yb^{3+}-doped hosts from $CsPbCl_3$ to $CsPbBr_3$ and deeply understand the related energy transfer mechanism. The change of sample color from white to yellow (Figure S18a,b), the red-shift of band-edge absorption (Figure S18c), and the extended decay lifetime for exciton recombination (Figure S18d) evidence the gradual substitution of Cl^- by Br^- in the $CsPbCl_3$ host. Indeed, the band-edge emission from PeNCs shows a tendency toward the low-energy region (Figure S18e), and the NIR emission from Yb^{3+} dopants is retained but remarkably decreases with the increase of the Br^- content in the host (Figure S18e) owing to energy mismatch during quantum cutting.[20] Notably, the shortened decay lifetime for 4f−4f transition of Yb^{3+} is attributed to the alteration of their crystal-field environment from $CsPbCl_3$ to

https://doi.org/10.1021/acsami.1c09421
ACS Appl. Mater. Interfaces 2021, 13, 34561−34571

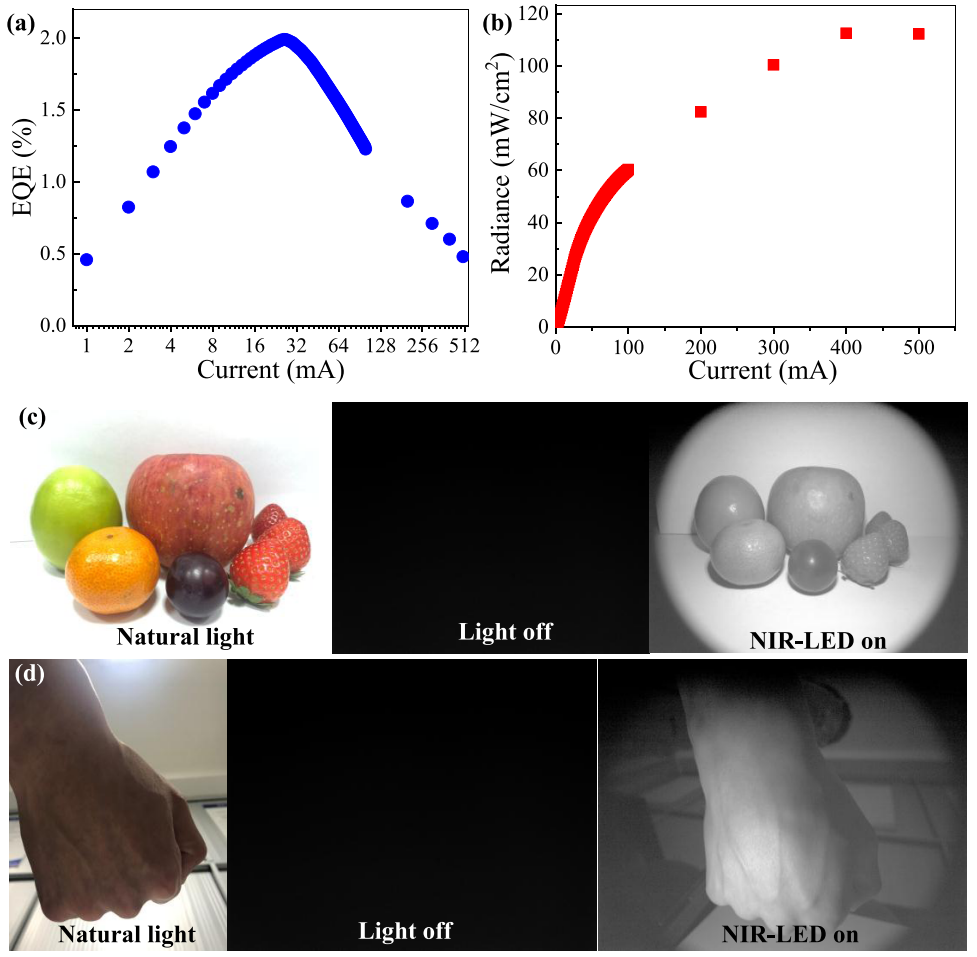

Figure 6. (a) EQE and (b) radiance of NIR emission from the constructed pc-NIR-LED versus forward bias current. Photographs of (c) fruits and (d) palm under natural light and pc-NIR-LED light recorded using the corresponding visible camera and NIR camera.

Table 1. Comparison of Optoelectronic Parameters of the EL-NIR-LED and pc-NIR-LEDs[a]

device	active size (mm)	current (mA)	voltage (V)	wavelength (nm)	peak EQE (%)	irradiance (mW/cm²)	references
EL-NIR-LED	3.0 × 3.0	~10	3.6	~1000	6	3.1	40
pc-NIR-LED1	3.0 × 3.0	815		~1000		3.5	41
pc-NIR-LED2	2.5 × 2.5	400	3.3	~1000	2	112	this work

[a]The emitting layers of pc-NIR-LED1 and pc-NIR-LED2 are Yb^{3+}-doped glass and Yb^{3+}:$CsPbCl_3$ quantum cutters, respectively.

$CsPbBr_3$ (Figure S18f). All of these results demonstrate the incorporation of Yb^{3+} dopants in $CsPb(Cl/Br)_3$ hosts and the necessity of energy match between the bandgaps of PeNCs and Yb^{3+} activator to achieve highly efficient NIR emission.

To explore the possible application of Yb^{3+}:$CsPbCl_3$ quantum cutters in NIR-LED devices, their thermal stability was investigated. Temperature-dependent PL spectra of Yb^{3+}:$CsPbCl_3$ recorded from RT (25 °C) to 240 °C are shown in Figures 5a and S19. It is found that NIR PL intensity at 110 °C can remain as high as 83% of the original one at RT and then quickly decreases upon further elevation of temperature (Figure 5b). At higher temperatures, the exciton recombination PL is remarkably quenched due to the low exciton binding energy of $CsPbCl_3$ PeNCs (Figure S20), which further affects PeNCs to Yb energy transfer-induced NIR luminescence. In a further experiment, the temperatures of 365 nm UV InGaN chips with the rated voltage of 10 V and varied currents were traced by the real-time infrared thermal images (Figure 5c). With the increase of the input current, it is clear that the actual temperature of the UV chips increase accordingly, reaching a value of ~94 °C with an operating power of 5 W. Fortunately, the NIR PL intensity of Yb^{3+}:$CsPbCl_3$ shows only ~15% loss at this temperature (Figure 5b), enabling their practical application as color converters in NIR-emitting pc-LEDs. The device is constructed by coupling 5 W UV commercial chips with Yb^{3+}:$CsPbCl_3$ quantum cutters with the help of A/B gels, which can produce bright NIR light collected by an industrial night-vision camera (inset of Figure 5d). The PLQY for the obtained Yb^{3+}:$CsPbCl_3$ embedded gel as the emitting layer can reach as high as ~115%. Notably, the commercial UV chips consist of 10 chips, and each chip requires only a low operating voltage of 3.3 V. The EL spectra of the operating device show one narrow UV emission assigned to the chip and the other broad NIR emission ascribed to Yb^{3+}:$CsPbCl_3$. Both UV and NIR emissions are enhanced monotonously with the increase of current from 1 to 500 mA (Figures 5d and S21),

https://doi.org/10.1021/acsami.1c09421
ACS Appl. Mater. Interfaces 2021, 13, 34561−34571

demonstrating that there is no obvious saturation toward the incident high-power (up to 5 W) UV light excitation.

The key optoelectronic parameters of the commercial UV LED chip (Figure S22) and the constructed pc-NIR-LED based on Yb^{3+}:$CsPbCl_3$ quantum cutters (Figure 6a,b) have been recorded and tabulated in Table 1. As a comparison, the related parameters for a recently reported electroluminescence NIR-LED (EL-NIR-LED) using Yb^{3+}:$CsPbCl_3$ PeQDs as the emitting layer are also listed in Table 1. The peak external quantum efficiency (EQE) for this EL-NIR-LED is 6% at a very low current of 0.075 mA, but its value will quickly decline with the increase of the input current (lower than 3% at 10 mA).[40] For our pc-NIR-LED, the peak EQE value for NIR emission reaches as high as ∼2% at a high current of 28 mA (Figure S23) and remains at ∼0.5% at 500 mA. Additionally, we have also fabricated the pc-NIR-LED with high content loading of Yb^{3+}:$CsPbCl_3$ PeNCs. As shown in Figure S24a, UV excitation light from the commercial UV chips can be completely converted into NIR light and the optimal EQE value is determined to be ∼1.5% (Figure S24b). This value is slightly lower than the best value of 2% (Figure 6b), which is probably ascribed to the reabsorption effect for the high-content Yb^{3+}:$CsPbCl_3$ emitters in the emissive layer. Importantly, the output irradiance (112 mW/cm^2) of pc-NIR-LED with an optimal current of 400−500 mA is about 35 times higher than that (3.1 mW/cm^2) of EL-NIR-LED.[40] It is worth noting that the present pc-NIR-LED exhibits superior long-term stability and its EL intensity shows no obvious change upon continuous operation for 24 h (Figure S25) since the emitting layer (Yb:$CsPbCl_3$ dispersed in epoxy resin) is quite stable and is excited by commercial stable UV chips. In addition, we also provide the optoelectronic parameters of the previously reported pc-NIR-LED using traditional Yb^{3+}-doped glass as the emitting layer.[41] Its EQE is not given and the output irradiance (3.5 mW/cm^2) is far lower than the value of the present device (112 mW/cm^2). All of these results confirm its high potential in practical applications.

Finally, we demonstrate a typical application of the present pc-NIR-LED in night-vision lighting. Figure 6c presents the photographs of fruits taken via different cameras (visible camera and NIR camera) under natural light and pc-NIR-LED light, respectively. When the pc-NIR-LED is off, no image can be captured by the NIR camera. In contrast, vivid black-and-white image is easily detected by NIR once the pc-NIR-LED lamp is lighted. A similar result can be obtained for photographs of the back of the palm and even the veins can be clearly observed after irradiation with the fabricated pc-NIR-LED (Figure 6d). These facts firmly demonstrate the application of the Yb^{3+}:$CsPbCl_3$ quantum cutters with real NIR emission in night-vision technologies, and other potential fields including food and medical industries can also be expected for this kind of NIR quantum cutting phosphor.

CONCLUSIONS

In summary, we report a novel hot-injection method to fabricate Yb^{3+}:$CsPbCl_3$ PeNCs using all metal-oleate salts as the cation precursors and TMS-Cl as the anion source. Yb^{3+} doping shows a saturation concentration of ∼7% and the optimal PLQY of Yb^{3+} NIR emission can reach as high as ∼110% owing to PeNC-sensitized cooperative energy transfer to two Yb^{3+} activators simultaneously in a picosecond time scale. The Yb^{3+}:$CsPbCl_3$ phosphor-converted NIR-LED exhibits a bright electroluminescence around ∼1000 nm with an EQE of 2% and a high radiance of 112 mW/cm^2, enabling it to find practical application in night-vision lighting.

ASSOCIATED CONTENT

Supporting Information

The Supporting Information is available free of charge at https://pubs.acs.org/doi/10.1021/acsami.1c09421.

Extra data pertaining to structural, spectroscopic, and LED device characterization, including STEM images, EDX mapping, absorption spectra, PL spectra, decay curves, PLQY, fluorescence images, TA spectra, EL spectra, EQE, and radiant flux of pc-NIR-LEDs (PDF)

AUTHOR INFORMATION

Corresponding Authors

Zhifang Li − *College of Photonic and Electronic Engineering, Fujian Normal University, Fuzhou 350117, China*; Email: lizhifang@fjnu.edu.cn

Xueyuan Chen − *CAS Key Laboratory of Design and Assembly of Functional Nanostructures, and Fujian Key Laboratory of Nanomaterials, Fujian Institute of Research on the Structure of Matter, Chinese Academy of Sciences, Fuzhou, Fujian 350002, China*; orcid.org/0000-0003-0493-839X; Email: xchen@fjnu.edu.cn

Daqin Chen − *Fujian Provincial Key Laboratory of Quantum Manipulation and New Energy Materials, College of Physics and Energy, Fujian Normal University, Fuzhou 350117, China; Fujian Provincial Collaborative Innovation Center for Advanced High-Field Superconducting Materials and Engineering, Fuzhou 350117, China; Engineering Research Center of Advanced Glass Manufacturing Technology, Ministry of Education, Donghua University, Shanghai 201620, China*; orcid.org/0000-0003-0088-2480; Email: dqchen@fjnu.edu.cn

Authors

Hai Huang − *Fujian Provincial Key Laboratory of Quantum Manipulation and New Energy Materials, College of Physics and Energy, Fujian Normal University, Fuzhou 350117, China*

Renfu Li − *CAS Key Laboratory of Design and Assembly of Functional Nanostructures, and Fujian Key Laboratory of Nanomaterials, Fujian Institute of Research on the Structure of Matter, Chinese Academy of Sciences, Fuzhou, Fujian 350002, China*

Shilin Jin − *Fujian Provincial Key Laboratory of Quantum Manipulation and New Energy Materials, College of Physics and Energy, Fujian Normal University, Fuzhou 350117, China*

Ping Huang − *CAS Key Laboratory of Design and Assembly of Functional Nanostructures, and Fujian Key Laboratory of Nanomaterials, Fujian Institute of Research on the Structure of Matter, Chinese Academy of Sciences, Fuzhou, Fujian 350002, China*

Jinquan Hong − *Fujian Key Laboratory of Functional Marine Sensing Materials, Minjiang University, Fuzhou 350108, China*

Shaowu Du − *Fujian Key Laboratory of Functional Marine Sensing Materials, Minjiang University, Fuzhou 350108, China*

Wei Zheng − *CAS Key Laboratory of Design and Assembly of Functional Nanostructures, and Fujian Key Laboratory of*

Nanomaterials, Fujian Institute of Research on the Structure of Matter, Chinese Academy of Sciences, Fuzhou, Fujian 350002, China; orcid.org/0000-0002-9651-0915

Complete contact information is available at: https://pubs.acs.org/10.1021/acsami.1c09421

Author Contributions

[▽]H.H. and R.L. contributed equally to this work.

Notes

The authors declare no competing financial interest.

■ ACKNOWLEDGMENTS

This research was supported by the National Natural Science Foundation of China (51972060, U1805252, and 51872048), the CAS/SAFEA International Partnership Program for Creative Research Teams, the Natural Science Foundation of Fujian Province (2020J02017), the Fujian Key Laboratory of Functional Marine Sensing Materials, Minjiang University (Grant No. MJUKF-FMSM202003), and the Fundamental Research Funds for the Central Universities (2232021G-07).

■ REFERENCES

(1) Ly, K. T.; Chen, R. W.; Lin, H. W.; Shiau, Y. J.; Liu, S. H.; Chou, P. T.; Tsao, C. S.; Huang, Y. C.; Chi, Y. Near-Infrared Organic Light-Emitting Diodes with very High External Quantum Efficiency and Radiance. *Nat. Photonics* **2016**, *11*, 63−68.

(2) Eggebrecht, A. T.; Ferradal, S. L.; Robichaux-Viehoever, A.; Hassanpour, M. S.; Dehghani, H.; Hershey, T.; Culver, J. P.; et al. Mapping Distributed Brain Function and Networks with Diffuse Optical Tomography. *Nat. Photonics* **2014**, *8*, 448−454.

(3) Zeng, B. B.; Huang, Z. Q.; Singh, A.; Yao, Y.; Abul, K.; et al. Hybrid Graphene Metasurfaces for High-Speed Mid-Infrared Light Modulation and Single-Pixel Imaging. *Light: Sci. Appl.* **2018**, *7*, No. 51.

(4) Qiao, J. W.; Zhou, G. J.; Zhou, Y. Y.; Zhang, Q. Y.; Xia, Z. G. Divalent Europium-Doped Near-Infrared-Emitting Phosphor for Light-Emitting Diodes. *Nat. Commun.* **2019**, *10*, No. 5267.

(5) Möller, S.; Katelnikovs, A.; Haase, M.; Jüstel, T. New NIR Emitting Phosphor for Blue LEDs with Stable Light Output up to 180 °C. *J. Lumin.* **2016**, *172*, 185−190.

(6) De Guzman, G. N. A.; Fang, M. H.; Liang, C. H.; Bao, Z.; Hu, S. F.; Liu, R. S. Near-Infrared Phosphors and Their Full Potential: A Review on Practical Applications and Future Perspectives. *J. Lumin.* **2020**, *219*, No. 116944.

(7) Rajendran, V.; Fang, M. H.; De Guzman, G. N.; Lesniewski, T.; Mahlik, S.; Grinberg, M.; Leniec, G.; Kaczmarek, S. M.; Lin, Y. S.; Lu, K. M.; Lin, C. M.; Chang, H.; Hu, S. F.; Liu, R. S. Super Broadband Near-Infrared Phosphors with High Radiant Flux as Future Light Sources for Spectroscopy Applications. *ACS Energy Lett.* **2018**, *3*, 2679−2684.

(8) Jia, Z. W.; Yuan, C. X.; Liu, Y. F.; Wang, X. J.; Sun, P.; Wang, L.; Jiang, H. C.; Jiang, J. Strategies to Approach High Performance in Cr^{3+}-Doped Phosphors for High-Power NIR-LED Light Sources. *Light: Sci. Appl.* **2020**, *9*, No. 86.

(9) Zhang, L. L.; Wang, D. D.; Hao, Z. D.; Zhang, X.; Pan, G. H.; Wu, H. J.; Zhang, J. H. Cr^{3+}-Doped Broadband NIR Garnet Phosphor with Enhanced Luminescence and its Application in NIR Spectroscopy. *Adv. Opt. Mater.* **2019**, *7*, No. 1900185.

(10) Huang, W. T.; Cheng, C. L.; Bao, Z.; Yang, C. W.; Lu, K. M.; Kang, C. Y.; Lin, C. M.; Liu, R. S. Broadband Cr^{3+}, Sn^{4+}-Doped Oxide Nanophosphors for Infrared Mini Light-Emitting Diodes. *Angew. Chem., Int. Ed.* **2019**, *58*, 2069−2072.

(11) Bai, B.; Dang, P.; Huang, D.; Lian, H.; Lin, J. Broadband Near-Infrared Emitting $Ca_2LuScGa_2Ge_2O_{12}$:Cr^{3+} Phosphors: Luminescence Properties and Application in Light-Emitting Diodes. *Inorg. Chem.* **2020**, *59*, 13481−13488.

(12) He, S.; Zhang, L. L.; Wu, H.; Wu, H. J.; Pan, G. H.; Hao, Z. D.; Zhang, X.; Zhang, L. G.; Zhang, H.; Zhang, J. H. Efficient Super Broadband NIR $Ca_2LuZr_2Al_3O_{12}$: Cr^{3+}, Yb^{3+} Garnet Phosphor for pc-LED Light Source toward NIR Spectroscopy Applications. *Adv. Opt. Mater.* **2020**, *8*, No. 1901684.

(13) Song, E. H.; Ming, H.; Zhou, Y. Y.; He, F. Q.; Wu, J. C.; Xia, Z. G.; Zhang, Q. Y. Cr^{3+}-Doped Sc-Based Fluoride Enabling Highly Efficient Near Infrared Luminescence: A Case Study of K_2NaScF_6: Cr^{3+}. *Laser Photonics Rev.* **2021**, *15*, No. 2000410.

(14) Fang, M. H.; Chen, K. C.; Majewska, N.; Lesniewski, T.; Mahlik, S.; Leniec, G.; Kaczmarek, S. M.; Yang, C. W.; Lu, K. M.; Sheu, H. S.; Liu, R. S. Hidden Structural Evolution and Bond Valence Control in Near-Infrared Phosphors for Light-Emitting Diodes. *ACS Energy Lett.* **2021**, *6*, 109−114.

(15) Zhou, X. F.; Geng, W. Y.; Li, J. Y.; Wang, Y. C.; Ding, J. Y.; Wang, Y. H. An Ultraviolet-Visible and Near-Infrared-Responded Broadband NIR Phosphor and Its NIR Spectroscopy Application. *Adv. Opt. Mater.* **2020**, *8*, No. 1902003.

(16) Wang, F.; Liu, X. G. Recent Advances in the Chemistry of Lanthanide-doped Upconversion Nanocrystals. *Chem. Soc. Rev.* **2009**, *38*, 976−989.

(17) Marin, R.; Jaque, D. Doping Lanthanide Ions in Colloidal Semiconductor Nanocrystals for Brighter Photoluminescence. *Chem. Rev.* **2021**, *121*, 1425−1462.

(18) Pan, G. C.; Bai, X.; Yang, D. W.; Chen, X.; Jing, P. T.; Qu, S. N.; Zhang, L. J.; Zhou, D. L.; Zhu, J. Y.; Xu, W.; Dong, B.; Song, H. W. Doping Lanthanide into Perovskite Nanocrystals: Highly Improved and Expanded Optical Properties. *Nano Lett.* **2017**, *17*, 8005−8011.

(19) Milstein, T. J.; Kroupa, D. M.; Gamelin, D. R. Picosecond Quantum Cutting Generates Photoluminescence Quantum Yields Over 100% in Ytterbium-Doped $CsPbCl_3$ Nanocrystals. *Nano Lett.* **2018**, *18*, 3792−3799.

(20) Milstein, T. J.; Kluherz, K. T.; Kroupa, D. M.; Erickson, C. S.; De Yoreo, J. J.; Gamelin, D. R. Anion Exchange and the Quantum-Cutting Energy Threshold in Ytterbium-Doped $CsPb(Cl_{1-x}Br_x)_3$ Perovskite Nanocrystals. *Nano Lett.* **2019**, *19*, 1931−1937.

(21) Vergeer, P.; Vlugt, T. J. H.; Kox, M. H. F.; der Hertog, M. I.; van der Eerden, J. P. J. M.; Meijerink, A. Quantum Cutting by Cooperative Energy Transfer in $Yb_xY_{1-x}PO_4$: Tb^{3+}. *Phys. Rev. B* **2005**, *71*, No. 014119.

(22) Zhang, Q. Y.; Yang, G. F.; Jiang, Z. H. Cooperative Downconversion in $GdAl_3(BO_3)_4$: RE^{3+}, Yb^{3+} (RE=Pr, Tb, and Tm). *Appl. Phys. Lett.* **2007**, *91*, No. 051903.

(23) Chen, D. Q.; Wang, Y. S.; Yu, Y. L.; Huang, P.; Weng, F. Y. Near-Infrared Quantum Cutting in Transparent Nanostructured Glass Ceramics. *Opt. Lett.* **2008**, *33*, 1884−1886.

(24) van der Ende, B.; Aarts, L.; Meijerink, A. Near-Infrared Quantum Cutting for Photovoltaics. *Adv. Mater.* **2009**, *21*, 3073−3077.

(25) Meijer, J. M.; Aarts, L.; van der Ende, B. M.; Vlugt, T. J. H.; Meijerink, A. Downconversion for Solar Cells in YF_3: Nd^{3+}, Yb^{3+}. *Phys. Rev. B* **2010**, *81*, No. 035107.

(26) Zhou, D. L.; Liu, D. L.; Pan, G. C.; Chen, X.; Li, D. Y.; Xu, W.; Bai, X.; Song, H. W. Cerium and Ytterbium Codoped Halide Perovskite Quantum Dots: A Novel and Efficient Downconverter for Improving the Performance of Silicon Solar Cells. *Adv. Mater.* **2017**, *29*, No. 1704149.

(27) Kroupa, D. M.; Roh, J. Y.; Milstein, T. J.; Creutz, S. E.; Gamelin, D. R. Quantum-Cutting Ytterbium-Doped $CsPb(Cl_{1-x}Br_x)_3$ Perovskite Thin Films with Photoluminescence Quantum Yields over 190%. *ACS Energy Lett.* **2018**, *3*, 2390−2395.

(28) Zhou, D. L.; Sun, R.; Xu, W.; Ding, N.; Li, D. Y.; Chen, X.; Pan, G. C.; Bai, X.; Song, H. W. Impact of Host Composition, Codoping, or Tridoping on Quantum-Cutting Emission of Ytterbium in Halide Perovskite Quantum Dots and Solar Cell Applications. *Nano Lett.* **2019**, *19*, 6904−6913.

(29) Luo, X.; Ding, T.; Liu, X.; Liu, Y.; Wu, K. F. Quantum-Cutting Luminescent Solar Concentrators Using Ytterbium-Doped Perovskite Nanocrystals. *Nano Lett.* **2019**, *19*, 338−341.
(30) Crane, M. J.; Kroupa, D. M.; Gamelin, D. R. Detailed-Balance Analysis of Yb3+: $CsPb(Cl_{1-x}Br_x)_3$ Quantum-Cutting Layers for High-Efficiency Photovoltaics under Real-World Conditions. *Energy Environ. Sci.* **2019**, *12*, 2486−2495.
(31) Hsu, B. W.; Chuang, Y. T.; Cheng, C. Y.; Chen, C. Y.; Chen, Y. J.; Brumberg, A.; Yang, L.; Huang, Y. S.; Schaller, R. D.; Chen, L. J.; Chuu, C. S.; Lin, H. W. Very Robust Spray-Synthesized $CsPbI_3$ Quantum Emitters with Ultrahigh Room-Temperature Cavity-Free Brightness and Self-Healing Ability. *ACS Nano* **2021**, DOI: 10.1021/acsnano.1c00733.
(32) Wang, J.; Deng, R.; MacDonald, M. A.; Chen, B.; Yuan, J.; Wang, F.; Chi, D.; Andy Hor, T. S.; Zhang, P.; Liu, G.; Han, Y.; Liu, X. G. Enhancing Multiphoton Upconversion through Energy Clustering at Sublattice Level. *Nat. Mater.* **2014**, *13*, 157−162.
(33) Duan, Q.; Qin, F.; Zhang, Z.; Cao, W. Quantum Cutting Mechanism in $NaYF_4$: Tb^{3+}, Yb^{3+}. *Opt. Lett.* **2012**, *37*, 521−523.
(34) Stręk, W.; Bednarkiewicz, A.; Deren, P. J. Power Dependence of Luminescence of Tb^{3+}-Doped $KYb(WO_4)_2$ Crystal. *J. Lumin.* **2001**, *92*, 229−235.
(35) Florêncio, L. D. A.; Gómez-Malagón, L. A.; Lima, B. C.; Gomes, A. S. L.; Garcia, J. A. M.; Kassab, L. R. P. Efficiency Enhancement in Solar Cells Using Photon Down-Conversion in Tb/Yb-Doped Tellurite Glass. *Sol. Energy Mater. Sol. Cells* **2016**, *157*, 468−475.
(36) Erickson, C. S.; Crane, M. J.; Milstein, T. J.; Gamelin, D. R. Photoluminescence Saturation in Quantum-Cutting Yb^{3+}-Doped $CsPb(Cl_{1-x}Br_x)_3$ Perovskite Nanocrystals: Implications for Solar Downconversion. *J. Phys. Chem. C* **2019**, *123*, 12474−12484.
(37) Diroll, B. T.; Zhou, H.; Schaller, R. D. Low-Temperature Absorption, Photoluminescence, and Lifetime of $CsPbX_3$ (X=Cl, Br, I) Nanocrystals. *Adv. Funct. Mater.* **2018**, *28*, No. 1800945.
(38) Roh, J. Y. D.; Smith, M. D.; Crane, M. J.; Biner, D.; Milstein, T. J.; Kramer, K. W.; Gamelin, D. R. Yb^{3+} Speciation and Energy-Transfer Dynamics in Quantum Cutting Yb^{3+}-Doped $CsPbCl_3$ Perovskite Nanocrystals and Single Crystals. *Phys. Rev. Mater.* **2020**, *4*, No. 105405.
(39) Li, X.; Duan, S.; Liu, H.; Chen, G.; Luo, Y.; Ågren, H. Mechanism for the Extremely Efficient Sensitization of Yb^{3+} Luminescence in $CsPbCl_3$ Nanocrystals. *J. Phys. Chem. Lett.* **2019**, *10*, 487−492.
(40) Ishii, A.; Miyasaka, T. Sensitized Yb^{3+} Luminescence in $CsPbCl_3$ Film for Highly Efficient Near-Infrared Light-Emitting Diodes. *Adv. Sci.* **2020**, *7*, No. 1903142.
(41) Fuchi, S.; Sakano, A.; Mizutani, R.; Takeda, Y. High Power and High Resolution Near-Infrared Light Source for Optical Coherence Tomography Using Glass Phosphor and Light Emitting Diode. *Appl. Phys. Express* **2009**, *2*, No. 032102.